JACS
JOURNAL OF THE AMERICAN CHEMICAL SOCIETY
ARTICLE
pubs.acs.org/JACS

Electrochemical and Structural Properties of a Protein System Designed To Generate Tyrosine Pourbaix Diagrams

Melissa C. Martínez-Rivera,[†] Bruce W. Berry,[†,‡] Kathleen G. Valentine,[†] Kristina Westerlund,[‡] Sam Hay,[‡] and Cecilia Tommos*[,†,‡]

[†]Graduate Group in Biochemistry & Molecular Biophysics and Department of Biochemistry & Biophysics, 905 Stellar-Chance Laboratories, University of Pennsylvania, Philadelphia, Pennsylvania 19104-6059, United States

[‡]Department of Biochemistry & Biophysics, Arrhenius Laboratories for Natural Sciences, Stockholm University, SE-106 91 Stockholm, Sweden

S Supporting Information

ABSTRACT: This report describes a model protein specifically tailored to electrochemically study the reduction potential of protein tyrosine radicals as a function of pH. The model system is based on the 67-residue α_3Y three-helix bundle. α_3Y contains a single buried tyrosine at position 32 and displays structural properties inherent to a protein. The present report presents differential pulse voltammograms obtained from α_3Y at both acidic (pH 5.6) and alkaline (pH 8.3) conditions. The observed Faradaic response is uniquely associated with Y32, as shown by site-directed mutagenesis. This is the first time voltammetry is successfully applied to detect a redox-active tyrosine residing in a structured protein environment. Tyrosine is a proton-coupled electron-transfer cofactor making voltammetry-based pH titrations a central experimental approach. A second set of experiments was performed to demonstrate that pH-dependent studies can be conducted on the redox-active tyrosine without introducing large-scale structural changes in the protein scaffold. α_3Y was re-engineered with the specific aim to place the imidazole group of a histidine close to the Y32 phenol ring. α_3Y-K29H and α_3Y-K36H each contain a histidine residue whose protonation perturbs the fluorescence of Y32. We show that these variants are stable and well-folded proteins whose helical content, tertiary structure, solution aggregation state, and solvent-sequestered position of Y32 remain pH insensitive across a range of at least 3−4 pH units. These results confirm that the local environment of Y32 can be altered and the resulting radical site studied by voltammetry over a broad pH range without interference from long-range structural effects.

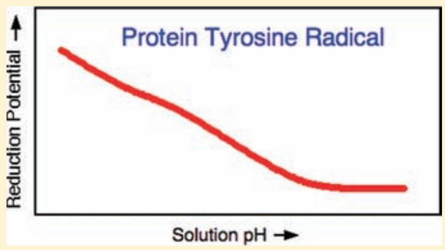

INTRODUCTION

Amino-acid radical enzymes use selected glycine, cysteine, tyrosine, and/or tryptophan residues as "in-house" one-electron redox cofactors.[1,2] Functional glycine and cysteine radicals tend to be generated near or at the active site and directly involved in the catalytic chemistry. The two aromatic residues are used in catalytic redox reactions as well as serving as intermediate components in radical-transfer chains spanning tens of Ångströms. Well-known examples of the former type are the Y_Z tyrosine in photosystem II (PSII)[3,4] and the cross-linked Tyr-His species in the active site of cytochrome *c* oxidase,[5] while the triple tryptophan electron-transfer wire in *E. coli* DNA photolyase,[6] the ~35 Å radical-transfer chain in *E. coli* ribonucleotide reductase (RNR),[7,8] and the putative multi-heme/tryptophan electron/radical transfer chain in the MauG/premethylamine dehydrogenase complex[9] represent examples of the latter type.

Virtually nothing is known as to how the protein matrix influences the thermodynamic properties of biocatalytic amino-acid radicals or the free-energy profiles of radical-transfer chains. It is very challenging to measure the reduction potentials of these highly oxidizing redox cofactors, and consequently, only a few estimates are available in the literature. An apparent potential of 1.0 V (pH 7.6) was reported for the tyrosine $Y-O^\bullet/Y-OH$-(122) redox pair in *E. coli* RNR,[10] although poor equilibria between the redox mediators in the bulk solvent and the radical site make this value unreliable. The formal potential of Y_Z in the large, membrane-bound PSII enzyme cannot be obtained directly by standard techniques such as redox titration or voltammetry-based methods, but a time-dependent "operating" potential has been estimated from kinetically derived equilibrium constants.[3,11] Assuming an operating potential of 1.25 V for $P_{680}{}^+/P_{680}$,[11,12] the $Y_Z-O^\bullet/Y_Z-OH$ potential falls between 1.13 and 1.22 V depending on the time elapsed after light excitation and the redox state of the adjacent Mn_4Ca cluster (pH 6.5 range; ref 13 and references therein). Likewise, an operating potential of 0.83 V (pH 6.0) has been estimated for the PSII $Y_D-O^\bullet/Y_D-OH$ redox couple.[11] These indirectly derived, single-pH potentials are, to our knowledge, the only available estimates for unmodified tyrosine radical cofactors. Even less is known about the potentials of protein glycine, cysteine, and tryptophan radical cofactors with experimental data available only for the

Received: July 22, 2011
Published: September 29, 2011

two-electron heme/W191 redox reactions in cytochrome *c* peroxidase[14] and the photolyase tryptophan−radical system.[15] Thus, on the basis of existing experimental data it is not possible to make any firm predictions regarding how the protein environment influences the reduction potentials of amino-acid radical cofactors. The hydrogen-bonding status of the reduced and radical states, the chemical characteristics of hydrogen-bonding partners, electrostatic interactions, solvent accessibility, and the effective dielectric of the protein environment are likely to play important roles,[3,16−19] but at present, correlations between these parameters and amino-acid radical reduction potentials are unknown and unexplored.

The thermodynamic properties of aqueous tyrosine give rise to a few key predictions regarding tyrosine redox chemistry in proteins.[2,3] The following half reactions, redox couples and acid dissociation constants are associated with tyrosine in water

$$\mathrm{Y{-}OH^{\bullet+} + e^- \Leftrightarrow Y{-}OH} \qquad \mathrm{Y{-}OH^{\bullet+}/Y{-}OH}$$

$$\mathrm{Y{-}O^{\bullet} + e^- + H^+ \Leftrightarrow Y{-}OH} \qquad \mathrm{Y{-}O^{\bullet}/Y{-}OH}$$

$$\mathrm{Y{-}O^{\bullet} + e^- \Leftrightarrow Y{-}O^-} \qquad \mathrm{Y{-}O^{\bullet}/Y{-}O^-}$$

$$\mathrm{Y{-}OH^{\bullet+} \Leftrightarrow Y{-}O^{\bullet} + H^+} \qquad K_{\mathrm{oY}} = [\mathrm{Y{-}O^{\bullet}}][\mathrm{H^+}]/[\mathrm{Y{-}OH^{\bullet+}}]$$

$$\mathrm{Y{-}OH \Leftrightarrow Y{-}O^- + H^+} \qquad K_{\mathrm{rY}} = [\mathrm{Y{-}O^-}][\mathrm{H^+}]/[\mathrm{Y{-}OH}]$$

The cation $\mathrm{Y{-}OH^{\bullet+}/Y{-}OH}$ redox couple dominates at pH below $\mathrm{p}K_{\mathrm{oY}}$, while the tyrosinate $\mathrm{Y{-}O^{\bullet}/Y{-}O^-}$ redox couple is observed at pH above $\mathrm{p}K_{\mathrm{rY}}$. There is no proton release or uptake associated with the change in redox state, and thus, the reduction potentials of the $\mathrm{Y{-}OH^{\bullet+}/Y{-}OH}$ and $\mathrm{Y{-}O^{\bullet}/Y{-}O^-}$ redox pairs are pH independent. The neutral tyrosine $\mathrm{Y{-}O^{\bullet}/Y{-}OH}$ pair is the dominant redox couple in the $\mathrm{p}K_{\mathrm{oY}} < \mathrm{pH} < \mathrm{p}K_{\mathrm{rY}}$ region. Since tyrosine oxidation/reduction is a $1e^-/1H^+$ event in this pH region, the potential follows the Nernst equation and decreases by 59 mV per pH unit at 25 °C. The $\mathrm{p}K_{\mathrm{oY}}$ and $\mathrm{p}K_{\mathrm{rY}}$ values are about −2 and 10 for aqueous tyrosine, respectively.[20] These values suggest that $\mathrm{Y{-}O^{\bullet}/Y{-}OH}$ is the dominant redox couple in a protein environment. Consequently, tyrosine oxidation/reduction reactions occurring inside proteins are expected to a large extent to involve proton-coupled electron transfer (PCET).

There are no electrochemical data of any kind available for a protein tyrosine radical, much less a full Pourbaix diagram representing the formal potential of this species over a significant pH range. The PCET characteristics of tyrosine and phenol redox systems predict that local interactions are critical for tuning their redox properties.[3,8,21] Thus, in order to obtain a meaningful Pourbaix diagram it is essential that the measured potential is not strongly influenced by global changes occurring in the protein scaffold as a function of pH but rather reflects local conditions at the radical site. We developed a tyrosine radical protein system that fulfills these criteria. The complexity of this task required a fairly extensive experimental approach including the use of voltammetry methods, protein design and engineering, absorption, fluorescence and CD spectroscopy, as well as several NMR-based techniques. The obtained data are described and analyzed in two connected papers. In the current paper we describe the electrochemical and structural properties of a protein system designed to provide tyrosine Pourbaix diagrams according to the criteria listed above. In a follow-up study, tyrosine Pourbaix diagrams obtained from this protein system are described and discussed.[22]

The tyrosine radical protein system is based on the de novo designed, 67-residue α_3Y three-helix bundle, which contains a single buried tyrosine at position 32 and originally no histidine residues.[16] In the present report we show that high-quality voltammetry data can be obtained from α_3Y at both acidic and alkaline conditions. We show that the observed Faradaic response is uniquely associated with Y32. This is the first time voltammetry is successfully applied to detect a redox-active tyrosine residing in a structured protein environment. We also demonstrate a high-level structural control over α_3Y by changing the environment of its redox-active tyrosine and proving that the resulting variants exhibit the required structural characteristics to support voltammetry-based pH titrations in a stable protein background. This is significant since pH-based studies are central to characterizing proton-coupled ET reactions in proteins. More specifically, α_3Y was re-engineered to make a histidine variant in which the imidazole ring of the introduced histidine interacts structurally with the phenol group of Y32. Our aim was to introduce an interaction at the site of the redox-active tyrosine and then specifically determine the effect of this interaction on the potential of Y32. This would demonstrate that the constructed tyrosine radical model system is capable of providing relevant radical site-specific information. Two variants of interest, α_3Y-K29H and α_3Y-K36H, were identified using protein modeling combined with optical and NMR-based spectroscopic screening. These two stable and well-structured proteins do not display any major changes in their secondary structures, tertiary structures, or solution aggregation state across a range of 3−4 pH units. Their single tyrosine residue Y32 is located in a hydrophobic and structured environment. Moreover, protonation of the introduced histidines perturbs the fluorescence of Y32, suggesting that α_3Y-K29H and α_3Y-K36H contain an electrostatically coupled Y32/His pair. We conclude that α_3Y-K29H and α_3Y-K36H exhibit the appropriate characteristics for probing the potential of Y32 as a function of local interactions and the solution pH.

■ MATERIALS AND METHODS

Protein Expression and Purification. The α_3Y proteins were made by QuikChange (Stratagene) using a modified α_3W/pET32b (Novagen) vector as template.[18] α_3Y has the following amino-acid sequence: GSRVKALEEKVKALEEKVKALGGGGRIEELKKKYEELK-KKIEELGGGGEVKKVEEEVKKLEEEIKKL in which the N-terminal GS residues form part of a thrombin cleavage site. These two residues are labeled as −2 and −1 to keep the amino-acid numbering consistent with the chemically synthesized 65-residue α_3Y protein.[16] α_3Y and variants were expressed in LB or minimal media and purified following standard protocols for His-tagged proteins (Novagen). Transformed BL21-(DE3)pLysS or BL21-CodonPlus(DE3)-RIL cells were harvested either after a 3−4 h IPTG induction period at 37 °C (LB cultures) or after an overnight induction at 30 °C (minimal media cultures) and stored at −20 °C. Cells were resuspended in 20 mM Tris-HCl, 500 mM NaCl, 5 mM imidazole, pH 7.9 and lysed by sonication. The lysate was clarified by centrifugation, passed over a His•bind (Novagen) nickel column, and the thioredoxin-α_3Y fusion protein eluted by an imidazole gradient. Thrombin (T6634; Sigma) was added to the thioredoxin-α_3Y protein fraction and the resulting mixture dialyzed against 50 mM Tris-HCl, 500 mM NaCl, 2.5 mM $CaCl_2$, pH 8.0 at room temperature overnight. The digestion mixture was passed over a second nickel column to remove the His-tagged thioredoxin and any remaining undigested fusion protein. Target proteins were isolated by reverse-phase HPLC (semipreparative TP2181010 column; Grace/Vydac) using an acetonitrile/water gradient containing 0.1% (w/v) trifluoroacetic acid and stored as lyophilized powder.

Absorption and Fluorescence Spectroscopy. Absorption spectra were collected on a Varian Cary 50 Bio or a Hitachi U-3000 UV/vis spectrometer at room temperature. pH-titration samples were prepared by dissolving lyophilized protein in a 10 mM potassium phosphate, 10 mM HEPES, 10 mM borate, 10 mM CAPS, pH 7.0 buffer to an Abs_{276} of 0.2 (10 mm path). The solution was split in two equal fractions and the pH carefully adjusted with 12 M HCl or 10 M NaOH. pH titrations were performed by constant volume titration. The apparent tyrosinate/tyrosine pK_a of Y32 was estimated by measuring at 293 nm (Abs_{max} for deprotonated Y32) and 400 nm (baseline) as a function of pH and fitting the resulting pH-titration curve to a single pK_a using the nonlinear curve-fitting routines in KaleidaGraph (www.synergy.com).

Fluorescence spectra were collected on a Horiba Jobin Yvon Spex Fluorolog spectrofluorometer at 23 °C. pH-titration samples were prepared by dissolving lyophilized protein in a 10 mM sodium acetate, 10 mM potassium phosphate, 10 mm sodium borate (APB), pH 7.0 buffer to an Abs_{276} of 0.2 (10 mm path), dividing the sample in two equal fractions, and adjusting the pH with either concentrated phosphoric acid or 10 M NaOH. The experiments were performed by constant volume titration and using λ_{ex} = 276 nm and λ_{em} = 285−445 nm. The slit width for the excitation and emission light was 0.7 and 2.0 nm, respectively, and the averaging time for each 0.05 nm step was 0.2 s. Tyrosine emission center of mass was calculated as described in ref 23 and the resulting pH-titration curves fitted to a single pK_a.

Circular Dichroism Spectroscopy. CD studies were conducted on an Aviv 202 CD spectrometer at 25 °C. For the α-helical measurements, lyophilized protein was dissolved in 10 mM APB pH 8.2 buffer to a concentration of ∼50 μM. To ensure accurate absorbance readings, the cuvette path length was 10 and 2 mm for the UV−vis and CD measurements, respectively. The absolute degree of secondary structures was determined by using α_3W as a reference (76 ± 1% α-helical between pH 4 and 10).[16,18] pH titrations were conducted by constant volume titration, and the samples were prepared by dissolving protein powder in 10 mM APB pH 7.0 buffer, splitting the solution into two equal fractions, and adjusting the pH with either 12 M HCl or 10 M NaOH. Chemical denaturation was conducted by automated constant volume titration of a 10 M urea protein sample into a 0 M urea protein sample. Samples were prepared by diluting protein stock in 10 mM APB pH 8.2 buffer containing either 0 or 10 M urea. The final protein concentrations were 15−40 μM for the pH and urea measurements. The degree of α-helical content and changes in this parameter were monitored by measuring the mean residue ellipticity at 222 nm ($[\Theta]_{222}$). The chemical denaturation curves were fitted as described in ref 24.

Size-Exclusion Chromatography. Gel filtration was performed using an analytical Superdex 75 column (GE Healthcare) equilibrated with 10 mM APB pH 7.0 buffer containing 100 mM KCl. The protein loading concentration was 250 μM.

NMR Spectroscopy. NMR data were collected using a Varian Inova 750 MHz spectrometer equipped with a conventional room temperature probe or a Bruker Advance III 750 MHz spectrometer fitted with a cryoprobe. pH-titration samples were prepared by dissolving lyophilized protein in a 10 mM deuterated sodium acetate, 10 mM sodium phosphate, 30 mM KCl, pH 4.0 buffer and in a 10 mM sodium phosphate, 10 mM sodium borate, 30 mM KCl, pH 10.0 buffer. Buffers were prepared in D_2O; all samples were ∼600 μM in protein and contained 500 μM 2,2-dimethyl-2-silapentane-5-sulfonate sodium salt (DSS) as a chemical-shift standard. pH titrations were conducted by equal volume titration and collecting one-dimensional (1D) spectra of the α_3Y-His proteins at 25 °C. The chemical shift of the imidazole ring Hε1 resonance[25] was used to determine the apparent imidazole/imidazolium pK_a values of the single histidine in the α_3Y-His proteins. Isotope effects were corrected using the following relationship: pK(H_2O) = 0.929 × pK(D_2O) + 0.42.[26] Two-dimensional (2D) ^{15}N-HSQC spectra[27] were obtained on ∼250 μM ^{15}N-labeled α_3Y-K29H and α_3Y-K36H dissolved in either 20 mM deuterated sodium acetate, 20 mM sodium phosphate, or 20 mM deuterated Tris. All samples contained 20 mM NaCl and 8% D_2O. ^{15}N-HSQC spectra were acquired at 25 and 35 °C using a spectral width of 14.0 ppm and 1024 complex points in the direct ^{1}H dimension and 18.0 ppm and 64 complex points in the indirect ^{15}N dimension. 2D ^{1}H−^{1}H NOESY spectra[28] were obtained on ∼200 μM α_3Y-K29H and α_3Y-K36H dissolved in D_2O containing 20 mM deuterated sodium acetate and 20 mM NaCl or 20 mM deuterated Tris and 20 mM NaCl. NOESY spectra were collected at 25 °C using a mixing time of 150 ms, a spectral width of 10.0 ppm, and 2048 complex points in the direct ^{1}H dimension and 10.0 ppm and 800 complex points in the indirect ^{1}H dimension. NMR data processing was performed with the Felix95 software (Accelrys Inc., San Diego, CA).

Electrochemistry. Cyclic voltammetry[29] and differential pulse voltammetry[29,30] were performed using an Autolab PGSTAT12 potentiostat. The electrochemical workstation was equipped with a temperature-controlled, Faraday-cage-protected three-electrode microcell (Princeton Applied Research) containing a Ag/AgCl reference electrode, a platinum wire counter electrode, and a 3 mm glassy carbon working electrode (all purchased from Advanced Measurements Inc.). The reference and counter electrodes were stored dry and routinely replaced after a limited set of experiments. They were prepared by filling the reference electrode with a 3 M KCl/saturated AgCl solution and the counter electrode with the buffer solution in which the sample was prepared. The surface of the working electrode was carefully polished between each measurement using a 0.05 μm alumina/water slurry on a glass-plate-mounted microcloth pad (Bioanalytical systems Inc.). The electrode was manually polished for 60 s, rinsed with water, sonicated first in ethanol for about 60 s and then in milli-Q water for another 60 s, and finally rinsed with an excess of Milli-Q water directed against the surface of the electrode. This protocol was repeated 2−3 times until a reproducible Faradaic response was observed from the sample. This cyclic procedure was typically performed only at the beginning of the experimental day, and once the working electrode was conditioned, only a single polish/sonicate/rinse step was required to activate the surface between measurements. Voltammetry measurements were performed immediately following the electrode-activation treatment. The performance of the assembled three-electrode cell was routinely checked by collecting differential pulse voltammograms from a standard sample containing 300 μM *N*-acetyl-tryptophanamide in 10 mM APB, 125 mM KCl, pH 3.0. All samples were prepared using ultrapure chemicals and the measurements made at 23 °C under an argon atmosphere. Data analysis was performed using the Autolab GPES software and PeakFit (Systat Software Inc.).

RESULTS

Voltammetry Studies of α_3Y. Panels A and B in Figure 1 show cyclic voltammograms of α_3Y and *N*-acetyl-L-tyrosinamide (NAYA), respectively. The two traces were obtained at very similar conditions, which are detailed in the figure legend. There is no observable Faradaic response from the protein sample, while the NAYA sample gives rise to an easily detectable anodic waveform. As expected,[31,32] the NAYA cyclic voltammogram is essentially completely irreversible. The poor response observed

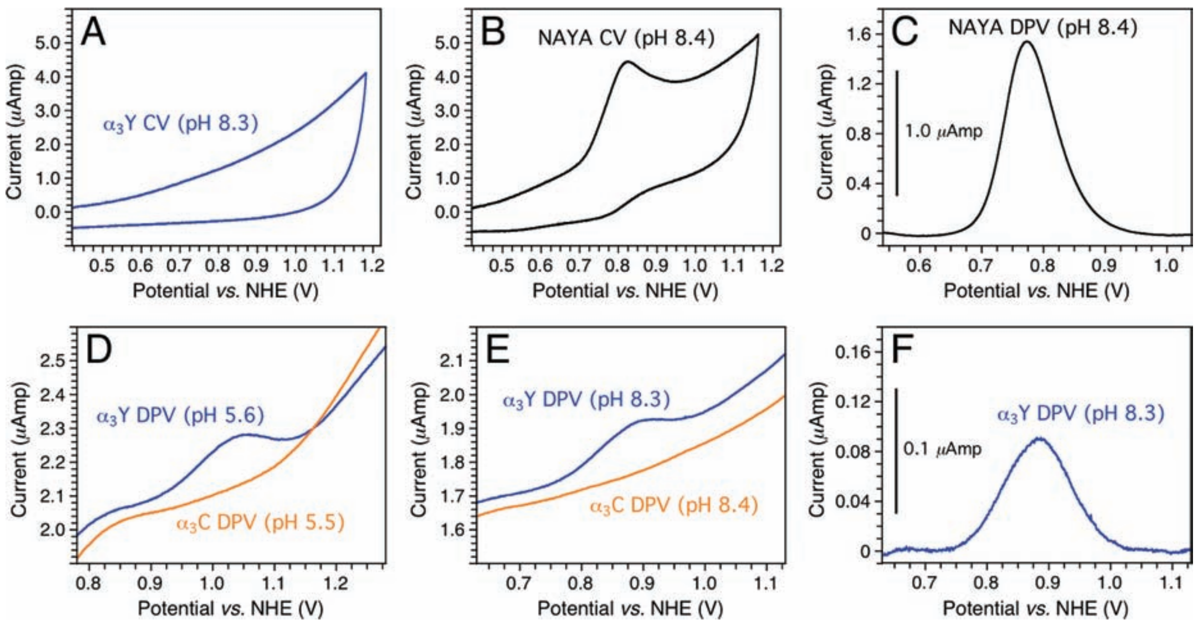

Figure 1. Electrochemical properties of α_3Y and control samples. (A) Cyclic voltammogram of 210 μM α_3Y in 20 mM potassium phosphate, 20 mM sodium borate, 40 mM KCl, pH 8.33; scan rate 200 mV/s, *iR*-compensation 103 ohm. (B) Cyclic voltammogram of 200 μM NAYA in 20 mM potassium phosphate, 20 mM sodium borate, 200 mM KCl, pH 8.37; scan rate 200 mV s^{-1}, *iR*-compensation 103 ohm. (C) Differential pulse voltammogram of 200 μM NAYA in 20 mM potassium phosphate, 20 mM sodium borate, 200 mM KCl, pH 8.37; interval time 0.1 s, step potential 1.05 mV, scan rate 10.5 mV s^{-1}, modulation time 8 ms, modulation amplitude 50 mV. The trace has been baseline corrected. (D) Differential pulse voltammograms of (blue) 210 μM α_3Y in 20 mM sodium acetate, 20 mM potassium phosphate, 40 mM KCl, pH 5.56, and (orange) 200 μM α_3C in 20 mM sodium acetate, 20 mM potassium phosphate, 40 mM KCl, pH 5.46; interval time 0.1 s, step potential 1.05 mV, scan rate 10.5 mV s^{-1}, modulation time 5 ms, modulation amplitude 50 mV. (E) Differential pulse voltammograms of (blue) 210 μM α_3Y in 20 mM potassium phosphate, 20 mM sodium borate, 40 mM KCl, pH 8.33, and (orange) 200 μM α_3C in 20 mM potassium phosphate, 20 mM sodium borate, 40 mM KCl, pH 8.45; interval time 0.1 s, step potential 1.05 mV, scan rate 10.5 mV s^{-1}, modulation time 8 ms, modulation amplitude 50 mV. (F) Baseline-corrected trace of the α_3Y differential pulse voltammogram shown in Figure 1E.

from α_3Y when using cyclic voltammetry could not be improved by changing the protein concentration, buffer conditions, or acquisition settings (e.g., see Figure S1A in the Supporting Information). Thus, unlike aqueous tyrosine[31] and aqueous phenol,[33] electrochemical analysis using cyclic voltammetry is at present not a feasible approach for the α_3Y system.

However, a significant Faradaic response could be obtained from α_3Y when using the more sensitive method of differential pulse voltammetry (DPV).[29,30] Panels D and E in Figure 1 show DP voltammograms obtained from α_3Y (blue) and α_3C (orange) at nearly identical conditions (see figure legend). α_3C is a redox-inert Y32C variant of α_3Y.[19] At both acidic (Figure 1D) and alkaline (Figure 1E) conditions α_3Y gives rise to a distinct oxidation wave while α_3C does not. Differential pulse voltammograms recorded on samples containing α_3C look essentially identical to baseline voltammograms collected on buffer samples (e.g., Figure S1B in the Supporting Information). We conclude that there is no Faradaic response from the three-helix bundle scaffold when Y32 is removed. Thus, the α_3Y voltammograms displayed in Figure 1D and 1E represent the unique tyrosine residing in the hydrophobic core of α_3Y.

Voltammograms obtained from aqueous samples at highly oxidizing potentials contain a prominent background current arising from water oxidation occurring at the surface of the working electrode. The magnitude of this current is influenced by the sample pH and by the type of working electrode used. Solvent oxidation effects are evident when comparing the raw and baseline-corrected α_3Y pH 8.3 voltammogram displayed in Figure 1E and 1F, respectively. α_3Y DP voltammograms obtained at both acidic and alkaline pH display near symmetric waveforms with a well-defined peak potential and a width at half height of ~125 mV.

Panels C and F in Figure 1 display baseline-corrected DPV traces of NAYA and α_3Y, respectively. These traces were obtained at comparable sample conditions and using identical acquisition parameters (see figure legend). The only significant difference was the KCl concentration, which was 40 mM in the protein sample and 200 mM in the NAYA sample. At lower salt concentration the NAYA voltammogram displayed characteristics consistent with electrode absorption. α_3Y gives rise to a current in the 0.1 μAmp range when using DPV, while the NAYA sample provides a current on the 1.0 μAmp range. Thus, the peak current of the Y32 voltammogram is about 1 order of magnitude smaller relative to the peak current obtained from freely solvated NAYA.

We conclude that high-quality tyrosine DP voltammograms can be obtained from α_3Y at both acidic and alkaline pH. The voltammogram collected at pH 5.6 is particularly impressive considering the high potential involved. Overall, these results represent the first successful use of voltammetry to detect a tyrosine radical located in a stable and well-folded protein environment. They also suggest that the α_3Y system can be used to obtain tyrosine Pourbaix diagrams spanning a significant pH range.

Protein Modeling. α_3Y was re-engineered to make a histidine variant displaying a detectable interaction between the imidazole ring of the introduced histidine and the phenol headgroup of

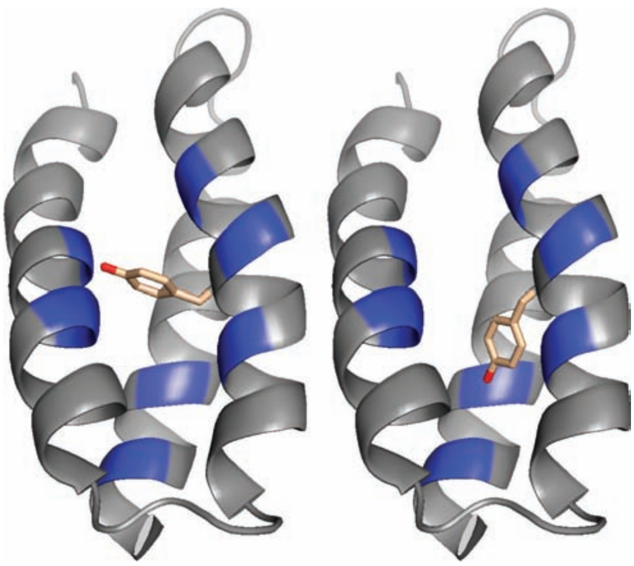

Figure 2. α_3Y models illustrating two possible orientations of the Y32 side chain. The α-carbons of residues changed in the α_3Y-His variants are shown in blue.

Y32. α_3Y is a W32Y variant of the structurally characterized α_3W three-helix bundle (see Figure S2 in the Supporting Information).[18] α_3Y and α_3W exhibit very similar structural properties including their α-helical content (~75%), pH stability (5−6 pH units), global stability (~ 4−5 kcal mol^{-1}), and solution aggregation state (monomeric).[16,18] Moreover, 2D ^{13}C-HSQC spectra reflecting the environment of protein core residues in these two proteins display comparable spectral line widths and chemical-shift dispersion. These observations show that large-scale structural changes do not occur in the three-helix bundle scaffold upon changing tryptophan 32 to a tyrosine. On this basis, α_3Y models with various Y32 χ^1 dihedral angles were made from the α_3W NMR structure[18] to identify sites where incorporation of a histidine could place the imidazole ring within 5 Å of the Y32 phenol oxygen (Figure 2). Histidine was modeled into each identified site, and a broad range of Y32/His χ^1 rotamer combinations were visually inspected. This analysis promoted generation of the following eight proteins: α_3Y-V9H, α_3Y-L12H, α_3Y-E13H, α_3Y-K29H, α_3Y-E33H, α_3Y-K36H, α_3Y-L58H, and α_3Y-I62H.

Screening for Y32/His Interactions in the α_3Y-His Variants. It is long known that the optical properties of phenols are sensitive to the dielectric and hydrogen-bonding properties of solvating molecules, e.g., ref 34. To provide an example, Figure S3A in the Supporting Information displays the absorption spectra of α_3Y (λ_{max} 277.8 nm) and NAYA (λ_{max} 275.3 nm) both obtained at neutral pH. The relative red shift of the α_3Y spectrum indicates that the Y32 side chain is shielded from the bulk solvent. This is consistent with other characteristics of Y32[16] and the sequestered position of the W32 residue (solvent-accessible surface area of 2.6 ± 1.4% across the α_3W NMR structural ensemble).[18,35] Absorption and fluorescence spectra of the eight α_3Y-His variants were compared to α_3Y spectra obtained at corresponding conditions to search for changes in the microenvironment of Y32. Only minor shifts were detected in the Y32 absorption (Figure S3B in the Supporting Information), while the fluorescence data provided more distinguishing information. We found α_3Y-E13H, α_3Y-E33H, and α_3Y-E58H excitation (data not shown) and emission (Figure S4 in the Supporting Information) spectra essentially identical to those of α_3Y, and these three proteins were excluded for further characterization. In contrast, excitation and/or emission spectra of α_3Y-V9H, α_3Y-L12H, α_3Y-K29H, α_3Y-K36H, and α_3Y-I62H are shifted relative to corresponding α_3Y spectra (Figure S5 in the Supporting Information), which prompted further studies of these five proteins.

Alterations in the optical properties of Y32 may arise from a local change in the vicinity of the aromatic residue but may also reflect a global perturbation of the protein scaffold. A second screening step was performed to probe the structural integrity of the five selected α_3Y-His proteins. pK_{app} values of Y32 and introduced histidines were determined optically via the tyrosinate absorbance at 293 nm (Figure S6 in the Supporting Information) and by following spectroscopically the NMR chemical shift of the imidazole ε1 proton (Figure S7 in the Supporting Information) as a function of pH. CD spectroscopy was used to determine absolute α-helical content, the pH sensitivity in this parameter, and global protein stability. Only a minor decrease in the degree of helicity was observed for α_3Y-V9H, α_3Y-K29H, and α_3Y-K36H relative to α_3Y (~5−10%; Figure 3 and Table 1). These proteins also give rise to well-defined unfolding/folding transitions (Figure S8A in the Supporting Information) from which the global protein stabilities could be determined (Table 1). In contrast, α_3Y-L12H and α_3Y-I62H show a loss of ~20% of their α-helical contents relative to α_3Y (Table 1) and give rise to poorly defined denaturation curves (Figure S8B in the Supporting Information). In addition, NMR resonances representing the H12 and H62 ring protons display relatively broad line widths. This effect was particularly pronounced for α_3Y-L12H with the imidazole Hε1 resonance broadened beyond detection between pH 6.3 and 7.4 (Figure 3C). These observations are all consistent with structurally perturbed protein folds, and no additional data were collected on α_3Y-L12H and α_3Y-I62H.

A key requirement for the tyrosine radical model system is that pH-induced structural changes in the protein scaffold do not obscure detection and characterization of local interactions at the radical site. Thus, for the histidine variants we wish to measure the potential of Y32 across the titratable pH range of the introduced histidine while avoiding large-scale structural changes. α_3Y-K29H and α_3Y-K36H meet this requirement well as they remain 66.8 ± 2.5% and 64.7 ± 0.8% α-helical, respectively, ±2 pH units around the pK_{app} values of H29 and H36 (Table 1). Although the CD and NMR data collected on α_3Y-V9H suggest a stable and well-folded protein, the pK_{app} of H9 is below the protein pH-stability range (Table 1). For this reason, α_3Y-V9H was excluded from further characterization.

Spectroscopic Evidence of Y32/His Interactions in α_3Y-K29H and α_3Y-K36H. Fluorescence pH titrations were conducted to probe for more direct evidence of Y32/His interactions in α_3Y-K29H and α_3Y-K36H. Figure 4A shows the α_3Y tyrosine emission center of mass as a function of pH. A 1.0 nm shift was observed between pH 5.1 and 9.1 and yielded a fitted single pK_{app} of 8.1 ± 0.1. This effect may arise from a pH-induced change in the electrostatic environment of the tyrosine, the hydrogen-bonding properties of the phenol OH group, or a combination thereof.[36] A more substantial shift of 4.3 nm was observed for α_3Y-K36H (Figure 4C). The pH-induced spectral changes titrate with a pK_{app} of 7.1 ± 0.1, which is equivalent to the pK_{app} value determined for H36 via NMR (Table 1). The correlation between the two pK_{app} values suggests that the Y32 fluorescence is sensitive to the protonation state of H36 and that the two aromatic side chains are in close proximity. Likewise, the

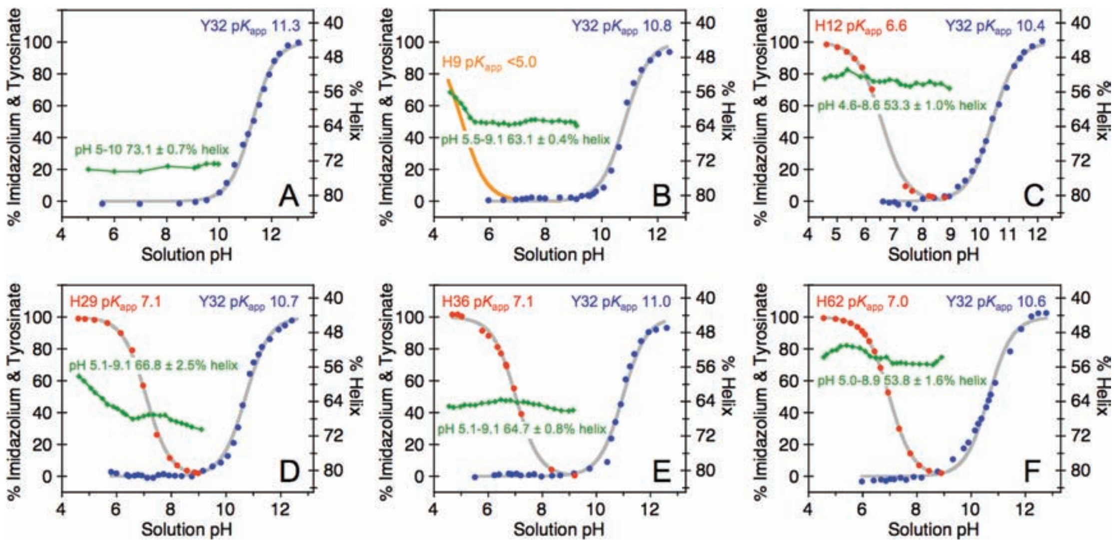

Figure 3. Physicochemical properties of α_3Y and single-site histidine variants. pH titrations of Y32 (blue circles) and histidine residues (red circles) are shown for (A) α_3Y, (B) α_3Y-V9H, (C) α_3Y-L12H, (D) α_3Y-K29H, (E) α_3Y-K36H, and (F) α_3Y-I62H. pK_{app} values were derived by nonlinear curve fitting (gray lines; Table 1). α-Helical contents as a function of pH are shown in green (diamonds).

Table 1. Physicochemical Properties of α_3Y and α_3Y-His Variants[a]

protein	pK_{app} Y32[b]	pK_{app} His[b]	Y32 Em(pH)[c]	$[\Theta]_{222}$[d]	% helix[e]	ΔG[f]
α_3Y	11.3		8.1	−21.9	73.1 ± 0.7 (pH 5.0−10.0)	−3.7
α_3Y-V9H	10.8	<5.0	n.d.	−18.7	63.1 ± 0.4 (pH 5.5−9.1)	−3.0
α_3Y-L12H	10.4	6.6	n.d.	−16.0	53.3 ± 1.0 (pH 4.6−8.6)	n.d.
α_3Y-K29H	10.7	7.1	7.4	−20.4	66.8 ± 2.5 (pH 5.1−9.1)	−2.8
α_3Y-K36H	11.0	7.0	7.1	−19.5	64.7 ± 0.8 (pH 5.1−9.1)	−2.4
α_3Y-I62H	10.6	7.0	n.d.	−16.5	53.8 ± 1.6 (pH 5.0−8.9)	n.d.

[a] Em (nm); $[\Theta]_{222} \times 10^3$ (deg cm^2 dmol^{-1}); ΔG (kcal mol^{-1}); n.d., not determined [b] Apparent tyrosinate/tyrosine and imidazole/imidazolium pK_a values of Y32 and histidine residues obtained by fitting the pH-titration curves in Figure 3 to a single pK_a. Statistical errors $\leq \pm 0.1$. [c] Apparent pK_a obtained by fitting the pH-titration curves in Figure 4 to a single pK_a. Statistical errors $\leq \pm 0.1$. [d] Mean residue ellipticity measured at pH 8.2 and 25 °C. The α_3W reference displays a $[\Theta]_{222}$ value of -22.6×10^3 deg cm^2 dmol^{-1} at the same conditions. [e] Scaled relative to α_3W (76 ± 1% α-helical pH 4−10).[16,18] [f] Global protein stabilities obtained by fitting the urea-denaturation curves in Figure S8A in the Supporting Information. Data recorded at pH 8.2 and 25 °C. Fitting standard errors < ± 0.03 kcal mol^{-1}.

α_3Y-K29H emission center of mass titrates with a pK_{app} of 7.4 ± 0.1 (Figure 4B). This value is similar to the NMR-derived H29 pK_{app} of 7.1 ± 0.1, suggesting a structural connection between Y32 and H29. The observed changes in the Y32 fluorescence most likely reflect electrostatic interactions between Y32 and the introduced histidine residues. Alternatively, changing the protonation state of the histidine leads to a change in the hydrogen-bonding environment of the Y32 OH group. Either of these explanations suggests that the imidazole group of the histidine residue introduced in α_3Y-K29H and α_3Y-K36H reside near or at the Y32 site.

Confirming the Absence of pH-Induced Changes in Aggregation State and Tertiary Structures. In preparation for voltammetry-based pH studies, it was essential to establish that α_3Y-K29H and α_3Y-K36H are monomeric and well structured across a significant pH range. Earlier work involving sedimentation equilibrium ultracentrifugation and analytical size-exclusion chromatography have demonstrated that the aggregation state of α_3Y in solution is that of a monomeric protein over a concentration range of at least 4−850 μM.[16] Moreover, 1D and 2D NMR spectra collected on α_3Y in the millimolar concentration range display characteristics consistent with a nonaggregated, uniquely folded protein. On the basis of these earlier observations, α_3Y was used here as a standard to determine the aggregation states of α_3Y-K29H and α_3Y-K36H. Figure S9 in the Supporting Information shows size-exclusion chromatograms obtained from α_3Y and α_3Y-K29H at pH 7.0 and a protein loading concentration of 250 μM. The α_3Y and α_3Y-K29H chromatograms display profiles consistent with a single major species (95% and 91% of the total 220 nm absorbance, respectively) eluting with a retention volume of 13.1 and 12.9 mL, respectively. An equivalent chromatogram obtained on α_3Y-K36H shows a single major species eluting at 13.1 mL (data not shown). We conclude that there are no significant differences in the hydrodynamic volume of the three proteins and, consequently, that they are all monomeric at neutral pH.

2D NMR spectroscopy was used to probe for changes in aggregation state and/or tertiary structure as a function of pH. ^{15}N-HSQC spectra were collected from α_3Y-K29H and α_3Y-K36H at three different pH values (5.5, 7.0, and 8.5) and two different temperatures (25 and 35 °C). Figure 5B shows the α_3Y-K29H ^{15}N-HSQC spectrum obtained at pH 7.0 and 25 °C.

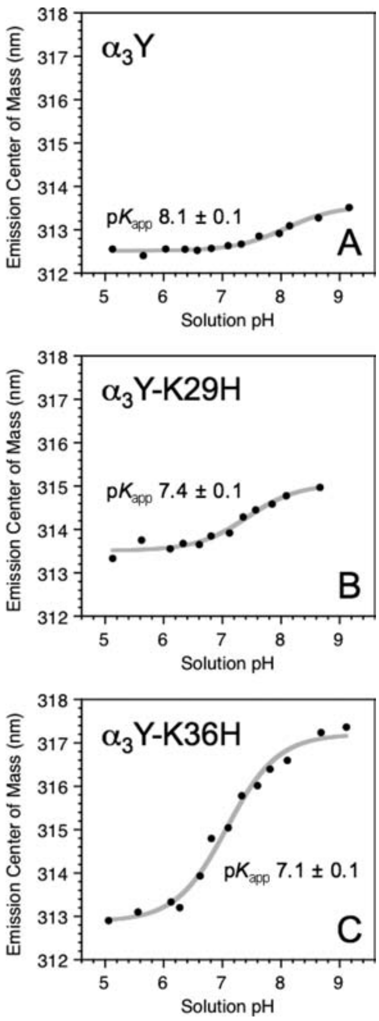

Figure 4. Fluorescence emission center of mass of Y32 in (A) α_3Y, (B) α_3Y-K29H, and (C) α_3Y-K36H as a function of pH. pK_{app} values were derived by nonlinear curve fitting (gray lines; Table 1).

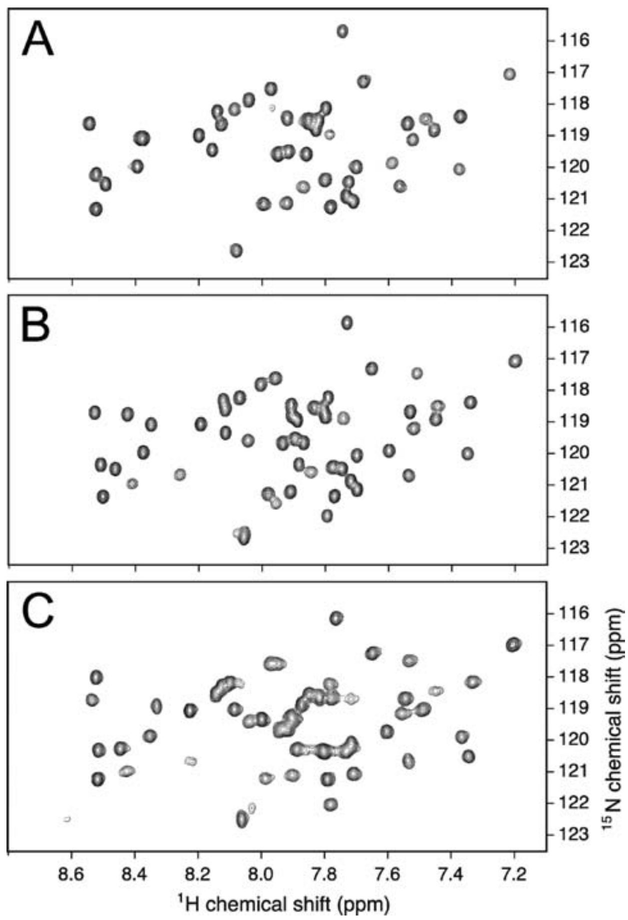

Figure 5. 2D ^{15}N-HSQC spectra of α_3Y-K29H obtained at 25 °C and with the pH at (A) 8.5, (B) 7.0, and (C) 5.5. These spectra, as well as those shown in Figure S10 in the Supporting Information, display a single set of peaks with no evidence of shadow peaks that would be indicative of minor conformers.

The displayed region of the 2D spectrum contains a set of 54 resolved ^{15}N$-$^{1}H cross peaks. In this spectral region we expect to detect ≤56 cross peaks arising from backbone N−H groups in the helical regions of the protein. Amide resonances associated with the eight glycines in loop regions (^{15}N 107−109 ppm) and L65 at the C-terminus (^{15}N 126.6 ppm) occur outside the displayed region. The observed narrow spectral line widths, overall chemical-shift dispersion, and absence of minor peaks confirm that α_3Y-K29H is a monomeric, uniquely folded protein at these conditions. Moreover, when comparing panels A, B, and C in Figure 5 it is clear that there are no significant changes in the spectral line widths as a function of pH, which, in turn, means that there is no significant change in the hydrodynamic volume of α_3Y-K29H. pH-induced electrostatic and hydrogen-exchange effects influence peak positions and intensities as expected, but the overall chemical-shift dispersion remains essentially the same. Thus, α_3Y-K29H remains well folded across the pH 5.5−8.5 range. The same conclusions can be made from the ^{15}N-HSQC pH 5.5, 7.0, and 8.5 spectra obtained from α_3Y-K29H at 35 °C (data not shown) and from α_3Y-K36H at 25 (data not shown) and 35 °C (Figure S10 in the Supporting Information). There are no significant changes in spectral line widths and chemical-shift dispersion as a function of protein, pH, and temperature. We conclude that α_3Y-K29H and α_3Y-K36H are monomeric and well-structured proteins across a pH range of at least 5.5−8.5.

Confirming That Y32 Is Buried in α_3Y-K29H and α_3Y-K36H. Figure 6 shows ^{1}H−^{1}H NOESY spectra obtained from α_3Y-K29H at pH 8.5 and 5.6 (Figure 6A and 6B) and α_3Y-K36H at pH 8.4 and 5.6 (Figure 6C and 6D). The selected region of the NOESY spectrum displays NOEs between the Y32 ring protons and aliphatic protons located within a distance of ∼5 Å. The δ1 and δ2 (the meta positions of the aromatic ring) and ε1 and ε2 (ortho positions) ring protons are unambiguously assigned on the basis of the observed intraresidue NOE patterns. For example, consider the α_3Y-K36H pH 8.4 spectrum (Figure 6C). The unresolved resonances of the δ1 and δ2 ring protons at 6.89 ppm show strong NOE correlations to the Y32 β protons at 2.99 and 3.15 ppm and Y32 α proton at 3.98 ppm. The unresolved resonances of the ε1 and ε2 ring protons at 6.76 also show intraresidue NOEs to the Y32 β and α protons but with weaker intensities corresponding to the longer ^{1}H−^{1}H distances. The same intraresidue Y32 NOE correlation patterns are observed in Figure 6A, 6B, and 6D.

Figure 6 shows that the Y32 ring protons are close to a dozen or more protons with resonances in the 0.59−0.97 ppm spectral region at both pH 8.5 and 5.6. The observed chemical shifts are

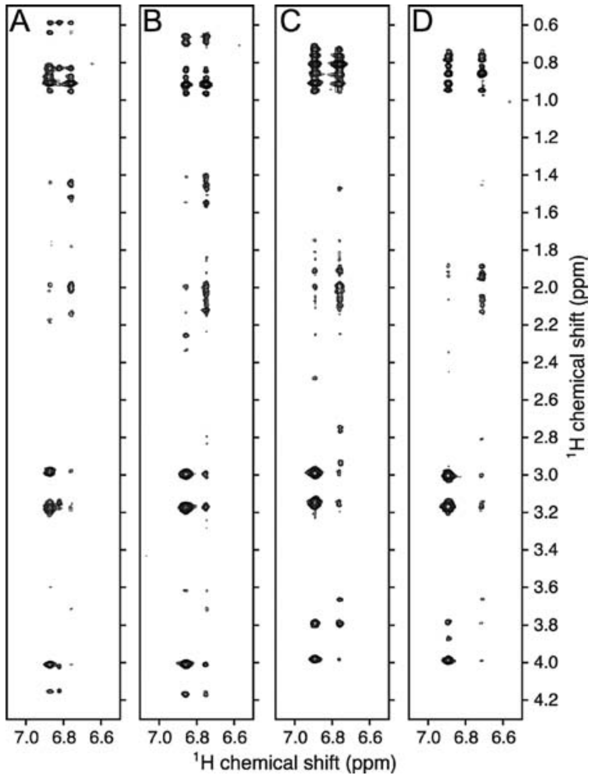

Figure 6. 2D ^{1}H−^{1}H-NOESY spectra obtained at 25 °C and representing (A) α_3Y-K29H at a measured pH of 8.5, (B) α_3Y-K29H at pH 5.6, (C) α_3Y-K36H at pH 8.4, and (D) α_3Y-K36H at pH 5.6.

consistent with resonances from methyl groups associated with valine, leucine, and isoleucine residues. These types of residues form the hydrophobic packing layers above, below, and at the level of W32 in the α_3W structure.[18,37] Depending on the pH, the α_3Y-K29H aromatic ring protons exhibit at least 12−26 additional inter-residue NOEs to aliphatic protons with resonances in the 1.40−4.17 ppm region (Figure 6A and 6B). For α_3Y-K36H at least 19−28 additional inter-residue NOEs are observed between the aromatic ring protons and nearby aliphatic protons (Figure 6C and 6D). These observations firmly suggest that Y32 is buried in the hydrophobic core of the two α_3Y histidine variants, as expected on the basis of the protein design and structural knowledge of α_3W.

■ DISCUSSION

Key Structural Properties of the Tyrosine Radical Protein System. Despite the fact that tyrosine radicals have been known to be involved in biological redox processes for more than three decades,[38] a basic Pourbaix diagram describing the reduction potential of a protein tyrosine radical as a function of the solution pH is not available. In fact, information regarding reduction potentials associated with protein tyrosine radicals is limited to only two indirectly derived, single-pH estimates (vide supra). This situation suggests that studies limited to the natural systems will not provide basic thermodynamic information of these essential PCET cofactors in a timely manner or even at all. For this reason, we adopted a model protein approach.

It is vital to stress that although the 7.5 kDa three-helix bundle scaffold used here is small relative to most naturally occurring tyrosine radical proteins, it nonetheless exhibits all of the key characteristics of a protein system. Its folding is driven by the hydrophobic effect.[18,35,37] Its unfolding/folding transition is reversible and cooperative (e.g., Figure S8A in the Supporting Information). Importantly, the ensemble of conformers that represents the solution state of the three-helix bundle proteins occupies narrow wells as shown by the excellent structural statistics of α_3W (see Figure S2 legend in the Supporting Information) and by the characteristics of their HSQC spectra (e.g., Figures 5 and S10 in the Supporting Information). Structural statistics of similar high quality were recently obtained for the NMR solution structures of two phenol-containing derivatives of α_3Y (unpublished data). Finally, the tyrosine of interest Y32 is desolvated and maintained in a highly structured environment across a broad pH range. These structural properties uniquely separate the model system described here from all other tyrosine/phenol radical model systems described thus far in the literature. In these small-molecule, e.g., ref 39, and peptide, e.g., refs 32 and 40, model systems, the phenol side chain resides in a highly solvent-exposed and dynamic environment.

Electrochemical Approach. Protein electrochemistry includes classic redox titrations using chemical titrants and a redox cuvette,[41] redox titrations using a thin-layer spectroelectrochemical cell controlled by a potentiostat,[42] and protein voltammetry.[43] Redox titrations require a mediator system that covers the potential range of interest and a distinct spectroscopic feature that reflects the redox state of the cofactor. The size and complexity of the redox protein generally do not provide an experimental barrier as long as the redox center is in equilibrium with the electrode via the redox mediators and give rise to a detectable signal that occurs outside the spectral envelope of the added mediators. In contrast, protein voltammetry does not require redox mediators or a spectroscopic probe of the redox system. This technique is however highly sensitive to the size of the protein and its orientation on the electrode surface since there must be electronic contact between the redox cofactor and the working electrode. The experimental time scale differs between the two approaches as redox titrations are conducted on the hours time scale while voltammetry data are typically collected on the minutes to millisecond time scale.

The main characteristics of α_3Y all suggest that voltammetry is the feasible approach. The small size of the protein is an advantage and predicts that a functional Y32/electrode electron-tunneling distance can occur in multiple α_3Y/electrode spatial orientations. α_3Y is a high-potential system, and an experimental time scale in the minutes rather than hours range reduces the risk of oxidative damage. Moreover, the weak optical features of α_3Y (ε_{276} 1490 M^{-1} cm^{-1} for reduced α_3Y, ε_{408} 2750 M^{-1} cm^{-1} for oxidized tyrosine[44]) combined with spectral overlap of redox mediators, typically used in the high-potential range,[10,45] will make spectroscopic monitoring of the α_3Y redox state challenging. Finally, and most importantly, voltammetry can provide kinetic and mechanistic information in addition to thermodynamic parameters.[33,43] Thus, the key demonstration of a reproducible Faradaic response from Y32 sets the stage for more detailed studies as we continue to develop the α_3Y system.

The main challenge in protein voltammetry is to identify a working electrode system that provides the potential range required, allows direct cofactor/electrode electron transfer, and promotes the folded protein to interact in a favorable manner with the electrode surface without adsorptive denaturation. A variety of electrode preparation strategies have been employed in order to modulate the strength of the protein/electrode interactions to, ideally, generate either a diffusion-controlled system or a stable protein film.[43]

Electrochemical Response of α_3Y. In this study, our first aim was to demonstrate that Y32 is redox active and that voltammetry can be used to probe the potential of the tyrosine in the folded protein at both acidic and alkaline conditions. A glassy carbon electrode was chosen as the working electrode system since it has an anodic potential window that extends to about +1.3 V vs NHE in aqueous media.[29] The glassy carbon electrode was activated by polishing the surface in an Al_2O_3/water slurry, which is predicted to generate a hydrophilic surface with C−O functionalities such as hydroxyls, carbonyls, ethers, and carboxylates.[46] In a preliminary study on α_3Y, a Faradaic response could not be obtained from the folded protein but only at sample conditions where the protein is unfolded.[16] By refining the pretreatment of the working electrode (see Materials and Methods section), we have now obtained differential pulse voltammograms from α_3Y at sample conditions where the protein is known to be monomeric, folded, and well structured. Once the electrode pretreatment protocol was obtained, the electrochemical response from α_3Y was compared at high and low pH, allowing sample conditions and acquisition parameters to be refined in an iterative manner, yielding typical voltammograms of the quality shown in Figure 1D−F. We showed that the Faradaic response is uniquely associated with Y32 and that it is abolished when the tyrosine is replaced by site-directed mutagenesis. Importantly, this is the first time voltammetry is successfully applied to detect a redox-active tyrosine residing in a structured protein environment.

Structural Properties of α_3Y-K29H and α_3Y-K36H. Our second major goal was to demonstrate that Pourbaix diagrams derived from the tyrosine radical protein system reflect the *local* environment of the redox-active tyrosine. Overall, this goal represents a quite challenging task and was divided into three connected projects including the following: (1) To engineer and demonstrate the presence of a specific structural interaction at the site of the redox-active tyrosine. (2) To demonstrate that the structural properties of the re-engineered α_3Y variants are appropriate in order to conduct voltammetry-based pH titrations. Thus, effects on the tyrosine radical potential from global events occurring in the protein scaffold, such as pH-induced changes in secondary and tertiary structures, must be minimized. In addition, the aggregation state of the protein should be pH independent to avoid a situation in which the distance between the radical site and the surface of the working electrode varies as a function of pH. This can lead to changes in the shape and position of the voltammogram representing the redox-active tyrosine and to an overall loss of the Faradaic signal.[47] (3) To derive potential vs pH diagrams from α_3Y and variants and determine the effects of the specifically engineered interaction on the tyrosine redox system. This study completes the first two objectives.

We re-engineered α_3Y with the specific aim to place the imidazole group of a histidine residue close to the phenol ring of Y32 (Figures 2 and S2 in Supporting Information). Eight α_3Y-His variants were generated of which two displayed promising spectroscopic and structural characteristics. α_3Y-K29H and α_3Y-K36H each contain a histidine residue whose protonation perturbs the fluorescence of Y32 (Table 1; Figure 4). This observation suggests that the engineered histidine and the redox-active Y32 residue are in close proximity. Moreover, we show that α_3Y-K29H and α_3Y-K36H are stable (Figure S8 in the Supporting Information; Table 1) and well-folded proteins whose α-helical content (Figure 3), tertiary structure (Figures 5 and S10 in the Supporting Information), solution aggregation state (Figures 5, S9, and S10 in the Supporting Information), and solvent-sequestered position of Y32 (Figure 6) are pH independent or highly pH insensitive across a range of at least 3−4 pH units. These results demonstrate that we achieved a tight structural control over the model protein hosting the redox-active tyrosine and that voltammetry measurements can be conducted across a broad pH range without large-scale structural changes occurring in the protein scaffold. Thus, the described model system is uniquely adapted to use voltammetry to study PCET reactions associated with tyrosine radical chemistry occurring in a solvent-sequestered and well-structured protein environment. Such studies are described in a separate report.[22]

■ ASSOCIATED CONTENT

Supporting Information. Figures showing cyclic and differential pulse voltammograms of α_3Y and control samples; the α_3W solution NMR structure; absorption and fluorescence spectra of NAYA, α_3Y, and single-site histidine variants; absorption spectra of α_3Y at neutral and high pH; 1D NMR spectra of α_3Y-K36H at acidic, neutral, and alkaline pH; denaturation plots of α_3Y and single-site histidine variants; size-exclusion chromatograms of α_3Y and α_3Y-K29H; ^{15}N-HSQC spectra of α_3Y-K36H. This material is available free of charge via the Internet at http://pubs.acs.org.

■ AUTHOR INFORMATION

Corresponding Author
*E-mail: tommos@mail.med.upenn.edu.

■ ACKNOWLEDGMENT

We are indebted to Drs. Josh Wand, Harry Gray, and Jeff Warren for extensive and valuable discussions. Funding was provided by NIH grant GM079190 and by NIH predoctoral fellowship GM096756 to M.C.M.R.

■ REFERENCES

(1) (a) Stubbe, J.; van der Donk, W. A. *Chem. Rev.* **1998**, *98*, 705–762. (b) Frey, P. A.; Hegeman, A. D.; Ruzicka, F. J. *Crit. Rev. Biochem. Mol. Biol.* **2008**, *43*, 63–88.

(2) Hoganson, C. W.; Tommos, C. *Biochim. Biophys. Acta* **2004**, *1655*, 116–122.

(3) Tommos, C.; Babcock, G. T. *Biochim. Biophys. Acta* **2000**, *1458*, 199–219.

(4) (a) Umena, Y.; Kawakami, K.; Shen, J.-R.; Kamiya, N. *Nature* **2011**, *473*, 55–60. (b) Kawakami, K.; Umena, Y.; Kamiya, N.; Shen, J.-R. *J. Photochem. Photobiol. B* **2011**, *104*, 9–18.

(5) (a) Proshlyakov, D. A.; Pressler, M. A.; DeMaso, C.; Leykam, J. F.; DeWitt, D. L.; Babcock, G. T. *Science* **2000**, *290*, 1588–1591. (b) Hemp, J.; Robinson, D. E.; Ganesan, K. B.; Martinez, T. J.; Kelleher, N. L.; Gennis, R. B. *Biochemistry* **2006**, *45*, 15405–15410. (c) Gorbikova, E. A.; Belevich, I.; Wikström, M.; Verkhovsky, M. I. *Proc. Nat. Acad. Sci. U.S.A.* **2008**, *105*, 10733–10737.

(6) Aubert, C.; Vos, M. H.; Mathis, P.; Eker, A. P. M.; Brettel, K. *Nature* **2000**, *405*, 586–590.

(7) (a) Sjöberg, B. M. *Struct. Bonding (Berlin)* **1997**, *88*, 139–173. (b) Stubbe, J.; Nocera, D. G.; Yee, C. S.; Chang, M. C. Y. *Chem. Rev.* **2003**, *103*, 2167–2202.

(8) Reece, S. Y.; Hodgkiss, J. M.; Stubbe, J.; Nocera, D. G. *Philos. Trans. R. Soc. B* **2006**, *361*, 1351–1364.

(9) Jensen, L. M. R.; Sanishvili, R.; Davidson, V. L.; Wilmot, C. M. *Science* **2010**, *327*, 1392–1394.
(10) Silva, K. E.; Elgren, T. E.; Que, L.; Stankovich, M. T. *Biochemistry* **1995**, *34*, 14093–14103.
(11) Rappaport, F.; Diner, B. A. *Coord. Chem. Rev.* **2008**, *252*, 259–272.
(12) Grabolle, M.; Dau, H. *Biochim. Biophys. Acta* **2005**, *1708*, 209–218.
(13) (a) Jeans, C.; Schilstra, M. J.; Klug, D. R. *Biochemistry* **2002**, *41*, 5015–5023. (b) Buchta, J.; Grabolle, M.; Dau, H. *Biochim. Biophys. Acta* **2007**, *1767*, 565–574.
(14) Mondal, M. S.; Fuller, H. A.; Armstrong, F. A. *J. Am. Chem. Soc.* **1996**, *118*, 263–264.
(15) Byrdin, M.; Lukacs, A.; Thiagarajan, V.; Eker, A. P. M.; Brettel, K.; Vos, M. H. *J. Phys. Chem. A* **2010**, *114*, 3207–3214.
(16) Tommos, C.; Skalicky, J. J.; Pilloud, D. L.; Wand, A. J.; Dutton, P. L. *Biochemistry* **1999**, *38*, 9495–9507.
(17) Tommos, C. *Philos. Trans. R. Soc. B* **2002**, *357*, 1383–1394.
(18) Dai, Q.-H.; Tommos, C.; Fuentes, E. J.; Blomberg, M. R. A.; Dutton, P. L.; Wand, A. J. *J. Am. Chem. Soc.* **2002**, *124*, 10952–10953.
(19) Hay, S.; Westerlund, K.; Tommos, C. *Biochemistry* **2005**, *44*, 11891–11902.
(20) Dixon, W. T.; Murphy, D. *J. Chem. Soc., Faraday. Trans. II* **1976**, *72*, 1221–1230.
(21) (a) Huynh, M. H. V.; Meyer, T. J. *Chem. Rev.* **2007**, *107*, 5004–5064. (b) Reece, S. Y.; Nocera, D. G. *Annu. Rev. Biochem.* **2009**, *78*, 673–699. (c) Warren, J. J.; Tronic, T. A.; Mayer, J. M. *Chem. Rev.* **2010**, *110*, 6961–7001. (d) Dempsey, J. L.; Winkler, J. R.; Gray, H. B. *Chem. Rev.* **2010**, *110*, 7024–7039.
(22) Berry B. W.; Martínez-Rivera, M. C.; Tommos, C. Submitted to the *Proceedings of the National Academy of Sciences U.S.A.*
(23) Ehrhardt, M. R.; Erijman, L.; Weber, G.; Wand, A. J. *Biochemistry* **1996**, *35*, 1599–1605.
(24) Santoro, M. M.; Bolen, D. W. *Biochemistry* **1988**, *27*, 8063–8068.
(25) Markley, J. L.; Bax, A.; Arata, Y.; Hilbers, C. W.; Kaptein, R.; Sykes, B. D.; Wright, P. E.; Wüthrich, K. *J. Mol. Biol.* **1998**, *280*, 933–952.
(26) Krezel, A.; Bal, W. *J. Inorg. Biochem.* **2004**, *98*, 161–166.
(27) Cavanagh, J.; Fairbrother, W. J.; Palmer, A. G.; Rance, M.; Skelton, N. J. *Protein NMR spectroscopy: Principles and practice*, 2nd ed.; Elsevier, New York, 2006.
(28) Jeener, J.; Meier, B. H.; Bachmann, P.; Ernst R. R. *J. Chem. Phys.* **1979**, *71*, 4546—4553.
(29) Bard, A. J.; Faulkner, L. R. *Electrochemical methods: Fundamentals and applications*, 2nd ed.; John Wiley & Sons, Inc.: New York, 2001.
(30) Parry, E. P.; Osteryoung, R. A. *Anal. Chem.* **1965**, *37*, 1634–1637.
(31) Harriman, A. *J. Phys. Chem.* **1987**, *91*, 6102–6104.
(32) DeFelippis, M. R.; Murthy, C. P.; Broitman, F.; Weinraub, D.; Faraggi, M.; Klapper, M. H. *J. Phys. Chem.* **1991**, *95*, 3416–3419.
(33) Costentin, C.; Louault, C.; Robert, M.; Savéant, J.-M. *Proc. Nat. Acad. Sci. U.S.A* **2009**, *106*, 18143–18148.
(34) (a) Strickland, E. H.; Wilchek, M.; Horwitz, J.; Billups, C. J. *J. Biol. Chem.* **1972**, *247*, 572–580. (b) Lee, J. K.; Ross, R. T. *J. Phys. Chem. B* **1998**, *102*, 4612–4618. (c) Noronha, M.; Lima, J. C.; Lamosa, P.; Santos, H.; Maycock, C.; Ventura, R.; Macanita, A. L. *J. Phys. Chem. A* **2004**, *108*, 2155–2166.
(35) Berry, B. W.; Elvekrog, M. M.; Tommos, C. *J. Am. Chem. Soc.* **2007**, *129*, 5308–5309.
(36) (a) Lakowicz, J. R. *Principles of Fluorescence Spectroscopy*; Plenum Press: New York, 1983. (b) Willis, K. J.; Szabo, A. G. *J. Phys. Chem.* **1991**, *95*, 1585–1589. (c) Lee, J. K.; Ross, R. T.; Thampi, S.; Leurgans, S. *J. Phys. Chem.* **1992**, *96*, 9158–9162.
(37) Westerlund., K.; Berry., B. W.; Privett, H. K.; Tommos, C. *Biochim. Biophys. Acta* **2005**, *1707*, 103–116.
(38) Sjöberg, B.-M.; Reichard, P.; Gräslund, A.; Ehrenberg, A. *J. Biol. Chem.* **1977**, *252*, 536–541.
(39) (a) Sjödin, M.; Styring, S.; Åkemark, B.; Sun, L.; Hammarström, L. *J. Am. Chem. Soc.* **2000**, *122*, 3932–3936. (b) Rhile, I. J.; Mayer, J. M. *J. Am. Chem. Soc.* **2004**, *126*, 12718–12719. (c) Benisvy, L.; Bittl, R.; Bothe, E.; Garner, C. D.; McMaster, J.; Ross, S.; Teutloff, C.; Nesse, F. *Angew. Chem., Int. Ed.* **2005**, *44*, 5314–5317. (d) Costentin, C.; Robert, M.; Savéant, J.-M. *J. Am. Chem. Soc.* **2006**, *128*, 4552–4553. (e) Markle, T. F.; Rhile, I. J.; DiPasquale, A. G.; Mayer, J. M. *Proc. Nat. Acad. Sci. U.S.A* **2008**, *105*, 8185–8190. (f) Moore, G. F.; Hambourger, H.; Kodis, G.; Michl, W.; Gust, D.; Moore, T. A.; Moore, A. L. *J. Phys. Chem. B* **2010**, *114*, 14450–14457. (g) Bonin, J.; Costentin, C.; Louault, C.; Robert, M.; Routier, M.; Savéant, J.-M. *Proc. Nat. Acad. Sci. U.S.A* **2010**, *107*, 3367–3372.
(40) (a) Sibert, R.; Jesowicz, M.; Porcelli, F.; Veglia, G.; Range, K.; Barry, B. A. *J. Am. Chem. Soc.* **2007**, *129*, 4393–4400. (b) Sibert, R.; Jesowicz, M.; Barry, B. A. *ACS Chem. Biol.* **2010**, *5*, 1157–1168.
(41) Dutton, P. L. *Methods Enzymol.* **1978**, *54*, 411–435.
(42) (a) Moss, D.; Nabedryk, E.; Breton, J.; Mäntele, W. *Eur. J. Biochem.* **1990**, *187*, 565–572. (b) Rich, P. R.; Iwaki, M. *Mol. Biosyst.* **2007**, *3*, 398–407.
(43) (a) Rusling, J. F. *Acc. Chem. Res.* **1998**, *31*, 363–369. (b) Armstrong, F. A.; Wilson, G. S. *Electrochim. Acta* **2000**, *45*, 2623–2645. (c) Armstrong, F. A. *Curr. Opin. Chem. Biol.* **2005**, *9*, 110–117.
(44) Feitelson, J.; Hayton, E. *J. Phys. Chem.* **1973**, *77*, 10–15.
(45) (a) Kálmál, L.; LoBrutto, R.; Allen, J. P.; Williams, J. C. *Nature* **1999**, *402*, 696–699. (b) Bellér, G.; Lente, G.; Fábián, I. *Inorg. Chem.* **2010**, *49*, 3968–3970.
(46) (a) Chen, P.; McGreery, R. L. *Anal. Chem.* **1996**, *68*, 3958–3965.(b) McGreery, R. L. In *Electrochemical properties of carbon surfaces, Interfacial chemistry*; Wiechowski, A., Ed.; Dekker: New York, 1999.
(47) (a) Nicholson, R. S.; Shain, I. *Anal. Chem.* **1964**, *36*, 706–723. (b) Laviron, E. *J. Electroanal. Chem. Interfacial Electrochem.* **1979**, *101*, 19–28. (c) Tender, L.; Carter, M. T.; Murray, R. W. *Anal. Chem.* **1994**, *66*, 3173–3181.